NASA/TM—2001-210819

Design Evaluation Using Finite Element Analysis of Cooled Silicon Nitride Plates for a Turbine Blade Application

Ali Abdul-Aziz
Cleveland State University, Cleveland, Ohio

George Y. Baaklini
Glenn Research Center, Cleveland, Ohio

Ramakrishna T. Bhatt
U.S. Army Research Laboratory, Glenn Research Center, Cleveland, Ohio

Prepared for the
103rd Annual Meeting and Exposition
sponsored by The American Ceramic Society
Indianapolis, Indiana, April 22–25, 2001

National Aeronautics and
Space Administration

Glenn Research Center

June 2001

Available from

NASA Center for Aerospace Information
7121 Standard Drive
Hanover, MD 21076

National Technical Information Service
5285 Port Royal Road
Springfield, VA 22100

Available electronically at http://gltrs.grc.nasa.gov/GLTRS

DESIGN EVALUATION OF COOLED SILICON NITRIDE PLATES USING FINITE ELEMENT ANALYSIS

Ali Abdul-Aziz,[1] George Y. Baaklini, and Ramakrishna T. Bhatt[2]
National Aeronautics and Space Administration
Glenn Research Center
Cleveland, OH 44135

ABSTRACT

Two- and three-dimensional finite element analyses were performed on uncoated and thermal barrier coated (TBC) silicon nitride plates with and without internal cooling by air. Steady-state heat-transfer analyses were done to optimize the size and the geometry of the cooling channels to reduce thermal stresses, and to evaluate the thermal environment experienced by the plate during burner rig testing. The limited experimental data available were used to model the thermal profile exerted by the flame on the plate. Thermal stress analyses were performed to assess the stress response due to thermal loading. Contours for the temperature and the representative stresses for the plates were generated and presented for different cooling hole sizes and shapes. Analysis indicates that the TBC experienced higher stresses, and the temperature gradient was much reduced when the plate was internally cooled by air. The advantages and disadvantages of several cooling channel layouts were evaluated.

INTRODUCTION

Engine manufacturers are continually attempting to improve the performance and efficiency of internal combustion engines. The thermal efficiency is typically improved by raising the operating temperature or reducing the cooling air requirement for the hot section turbine components Furthermore, lightweight, strong, tough high-temperature materials are required to complement efficiency improvements for next-generation gas turbine engines that can operate with minimum cooling.

Because of their low density, high-temperature strength, and thermal conductivity, ceramics are being investigated as potential materials for

[1] Cleveland State University, NASA Glenn Resident Research Associate.
[2] U.S. Army Research Laboratory, NASA Glenn Research Center.

replacing nickel-base alloys and superalloys that are currently used for engine hot-section components. Ceramic structures can withstand higher operating temperatures and a harsh combustion environment. In addition, their low densities relative to metals help reduce component mass (ref. 1).

The long term objectives of the project are to develop manufacturing technology, thermal environmental barrier coatings (TBC/EBC), and analytical modeling capability to predict thermo-mechanical stresses in minimally cooled silicon nitride turbine nozzle vanes under simulated engine conditions. In this preliminary study, finite element (FE) analyses were performed to calculate the thermo-mechanical stress response experienced by flat plate specimens made of silicon nitride. Two- and three-dimensional analyses with TBC were conducted. Nondestructive evaluation (NDE) was used to determine processing defects.

ANALYTICAL PROCEDURE

Parametric studies via finite element, heat transfer, and stress analyses were performed under steady-state conditions to demonstrate the feasibility of using cooled Si_3N_4 parts for turbine applications. The cross-sectional geometries of prototype silicon nitride plates with cooling holes used for FE analysis are shown in figure 1(a) and (b). In figure 1(a) the cooling hole dimensions remained the same, whereas in figure 1(b) the cooling hole dimensions were varied. Both plates consist of a top layer of zirconia, an intermediate layer of mullite, and a bond coat layer of reaction bonded silicon nitride (RBSN). Typical thicknesses of the top, intermediate, and bond coat layers are indicated in figure 1(a). Influence of cooling channel shapes, such as circular, square, rectangular, and variable geometry channels, on cooling efficiency and thermal stresses were investigated. Moreover, the thermal model considered for the analyses closely simulated impingement heating applied on the plate by the burner rig flame during the experiment. The hot flame was pointed symmetrically at the center region, which resulted in modeling half the plate. Temperature distributions were generated for all cases considered. The following paragraphs describe the analytical procedure employed.

Finite Element Analysis

Steady-state heat transfer analyses were conducted on the silicon nitride plates with and without internal cooling by air in a simulated burner rig testing condition. Figures 2(a) and (b) show an optical micrograph of the cross section of a silicon nitride plate fabricated with cooling channels and its radiographic image. The CT image indicates nonuniformity in cooling hole shape and spacing. In addition, it shows notable cracks in the cooling hole walls for some sections. It is coated with mullite and ZrO_2 thermal barrier

coatings, and it has the following dimensions: a thickness of 1.27 mm, a width of 36.10 mm, and a length of 33.53 mm. Physical properties of coatings employed in these analyses are given in table I (refs. 2 to 4).

Table I. Physical, mechanical, and thermal properties of materials

Material	Temperature, °C	Elastic modulus, GPa	Poisson's ratio	Coefficient of thermal expansion, $\times 10^{-6}$/°C	Thermal conductivity, K, W/m-k	Density, g/cm^3
Norton Si_3N_4 HS-130 (ref. 2)	25	300	0.22	3.3	30	3.1–3.2
	1400	250	0.19	3.3	12	3.1–3.2
RBSN (ref. 2)	25	70	0.18	3.5	5	1.6–1.92
RBSN (ref. 2)	1400	70	0.13	3.5	3	1.6–1.92
RBSN (ref. 2)	25	0.002–0.0034	0.25	11.25	0.2	0.59–1.12
Porous zirconia (ref. 3)	1400	0.002–0.0034	0.25	11.25	0.5	0.59–1.12
Mullite $3Al_2O_3 2SiO_2$ (ref. 4)	25	145	0.2	5.3	0.014	3.23
	1400	145	0.2	5.3	0.009	3.23

Various cooling channel sizes and specimen shapes were analyzed in an attempt to optimize a configuration that would offer a desirable thermal response under current assumed operating conditions. Figures 3(a) to (d) represent a series of two- and three-dimensional finite element models. Two different cooling channel configurations, circular and rectangular with equal sides (fig. 3(b)), were considered. The finite element models were generated with MSC/PATRAN graphics (ref. 5), and the analyses were performed using both MARC (ref. 6) and ANSYS (ref. 7) finite element codes.

Figure 3(c) represents the three-dimensional finite element model of the cooling plate panel specimen shown in figure 2. It consists of 8,372 eight-node hex elements and 13,568 nodes. The modeling assumed the geometric entities of the plate as represented in the computed tomography image, which included 28 near-oval-shape cooling channels. However, the existing oval cross sections were substituted with rectangular segments to simplify the model. A

proposed conceptual design shown in figure 1(b) was constructed to complement various hole sizes and to offer experimental flexibility in instrumenting small diameter test thermocouples for temperature measurements. Figure 3(d) shows the finite element model. It consists of 21,546 nodes and 17,760 hex eight-node elements. The modeling accounted for all the geometric variations indicated. Three-dimensional analyses were done to enable better understanding and to achieve broader coverage of the anticipated thermal profile under three-dimensional loading conditions.

Heat Transfer Analysis

The thermal boundary conditions applied were fundamental in evaluating the thermal profile predicted by the analyses. Several assumptions were made to model the heat transfer phenomena experienced by the test specimen. Related testing conditions were also simulated accordingly. Furthermore, convective boundary conditions were assumed and applied, and the corresponding heat transfer coefficients were obtained from reference 8. These handbook values were used because of the lack of requisite information concerning the fluid flow and the complete temperature environment experienced by the plate.

Figures 4(a) and (b) demonstrate the thermal boundary conditions applied for each analytical condition considered in the analyses.

Two-dimensional analysis: A slice from the middle section of the specimen plate was chosen for the analysis. The boundary conditions applied were imposed as follows (fig. 4(a)):

(1) As noted in figure 4(a), the top portion of the specimen was divided into two separate sections, with the center region as the first section, and the remaining part of the plate as the second. An impingement heating forced-convection heat transfer state was imposed to account for the heat transfer between the top surface of the plate and the hot gas exerted by the flame. A heat transfer coefficient value of 883 W/m^2-°C along with a gas temperature of 1982 °C was used to simulate the burner rig conditions and this process. This value of heat transfer coefficient corresponds well with values of heat transfer coefficients for superheated steam or air under forced convection state (ref. 8), which are highly representative of data used for the impingement heating environment.

(2) On the second section, a convective heat transfer coefficient of 6 W/m^2-°C was applied, a value that represents the free convection state used for the analysis. The gas temperature was linearly tapered off across the plate from a high of 1982 °C until it reached 700 °C.

(3) Cooling channels and the specimen bottom side were modeled with a convective heat transfer coefficient of 114 W/m^2-°C, a value for water cooling

in a forced convection state (ref. 8) and a gas temperature of 700 °C.

(4) Symmetry boundary conditions were imposed at the specimen midregion since only half the specimen was considered for the analyses.

(5) All coating effects were included in the two-dimensional analyses; layers of elements representing the coatings in the order described in figure 1(a) were generated.

Three-dimensional analysis: Figure 4(b) represents a view for the distribution of the thermal boundary conditions applied for this analytical case. Note that the topside of the specimen is split into three different sections, each simulating a specific environment. The center part simulates the impingement heating convective boundary conditions between the hot gas and the specimen surface with a heat transfer coefficient of 883 W/m^2-°C and a gas temperature of 1982 °C. The top inner sections above the entering and the existing flow of the cooling air were modeled by applying a convective coefficient of 883 W/m^2-°C and a gas temperature of 700 °C.

The sides of the specimen were assigned a heat transfer coefficient of 6 W/m^2-°C, and the corresponding gas temperature remained at 700 °C. A convective heat transfer coefficient value of 114 W/m^2-°C was used for the cooling channels and the bottom side of the specimen. However, the sink temperatures were as follows: 700 °C for the bottom side, 25 °C for the cooling air at the channel inlets, and 700 °C through the channels. A free convection state was assumed for the plate sides and bottom surface. Coating effects were included such that the first layer was porous zirconia and the second was mullite bond coating. This applies to all the two-dimensional models, as well as to the three-dimensional model shown in figure 3(d), except for the specimen shown in figure 1 where no coating was applied.

RESULTS AND DISCUSSION

Figures 5 to 10 show contour plots of temperature and stresses for all the analytical situations considered.

Figure 5(a) illustrates the temperature distribution generated via the finite element analysis conducted with the ANSYS code (ref. 7). It represents the cooling panel for the circular cooling hole geometry with a hole radius of 1.143 mm. The temperature variation is distributed over a range of 902 to 1371 °C, with the maximum temperature being at the middle section of the plate facing the flame. This was expected since the middle section of the plate is directly exposed to the flame temperature. Another observation can be made by noticing that the thermal barrier coating proved to limit the high-temperature profile to a thin layer of the plate because of conductivity

effects. As projected, the lowest temperature was recorded near the far edge of the plate away from the flame.

Figure 5(b) shows another case of the same geometry with larger cooling holes. The analytical conditions were kept similar to those reported in figure 5(a) except for the size of the cooling hole, which had a 1.524-mm radius. The pattern of temperature distribution and magnitude range was similar to that for the previous case (fig. 5(a)). However, the top hot spot was over a larger section than that for the smaller hole. Larger cooling channels will provide a higher cooling rate and will lead to the shorter distance between the topside and the cooling channel wall. Furthermore, the plate temperature was lower over a much wider surface area than it was for the plate containing smaller channels.

Figures 6(a), (b), and (c) show ANSYS results for the temperature distribution obtained for two different cases for the cooling plate panel with a rectangular cooling channel configuration. The plate had two different cooling channel sizes, 1.559 and 1.871 mm, respectively. Similar to the circular channel cases, the analyses were conducted with coolant and without coolant. The outcome, as shown in figures 6(a) and (b), illustrates that the temperature responded to the cooling effects as anticipated and that when cooling was used the temperature dropped about 204 °C from that for no-cooling boundary conditions. This supports the fact that applying coolant is highly effective in minimizing the temperature gradient and in reaching a desired lower level. Figure 6(c) shows the temperature profile under a different cooling channel size, 1.871 mm. As noted, the larger size channel without cooling effects increased the hotter area size substantially in comparison to the data reported in figure 6(a). This indicates that a larger cooling channel size is effective only when coolant is employed. Otherwise, it will lead to a higher surface temperature and, thus, a sizable thermal gradient.

Comparisons of hole size effects on the temperature are listed in figures 7(a) and (b) for the circular-shaped holes. The data presented are for two different spots on the plate, the locations of these spots are shown in figure 3(b). The hot point is on the top, and the cold point is on the bottom of the plate. As noted, the temperature climbs higher as the hole size grows larger for the without-cooling case, whereas it turns lower for the with-cooling case for the same hole size. This confirms that the temperature magnitude is highly dependent on both the hole size and the coolant. In addition, the temperature is substantially lower with both larger hole size and coolant, about 13 to 25 percent lower depending on the location.

Figures 8(a) and (b) show a three-dimensional contour of the temperature distributions for the cooling plate panel presented in figure 2. In these contours, the temperature is the highest at the center of the plate and it is

uniformly distributed across both the inlet and outlet sections. The hot temperature region became smaller when coolant was introduced, as noted in figure 8(b). This was an anticipated event, and it further confirms the added benefits of internally cooling the plate with air.

Figures 9(a) and (b) illustrate the temperature obtained as a result of the three-dimensional finite element analyses for the panel with incrementally increasing cooling channels. It can be seen from these two figures that, in contrast to the other layouts, the temperature level did not exceed 1204 °C. Furthermore; a temperature drop of near 93 °C demonstrates the effectiveness of the coolant (fig. 9(b)). The hot spot remained at the central portion of the plate as expected, and the inlet and outlet sections showed relatively uniform temperature profiles.

Table II shows the magnitude of the maximum and minimum temperature obtained for the plates under air cooling. Each channel cross-sectional shape delivered a different temperature; however, the two-dimensional analyses for circular and rectangular holes produced close results. Moreover, the model of the panel with incrementally increasing channels experienced the lowest temperature. A difference of near 260 °C was found among the three cooling hole configurations investigated. This can be attributed to the fact that the configuration with incrementally ascending channels is more suited to the thermal environment required by the experiment. Furthermore, it should be noted here that the smallest hole size in the ascending order configuration is equivalent in dimensions to those of the circular and rectangular configurations.

Table II. Temperature variation as a function of cooling channel cross sections with air cooling

Cooling channel shape	Temperature, °C	
	Maximum	Minimum
Rectangular	1344	976
Circular	1379	1068
Incrementally increasing square holes	1077	602

Figures 10(a) and (b) represent the contour plots of the maximum principal stress distributions generated for the incrementally ascending channels configuration. These plots were derived from a stress analysis conducted under thermal loading conditions predicted via a prior heat-transfer analysis. The plate was constrained to simulate the testing conditions of the experiment. At the coolant inlet side, the nodes at the one-third section of the plate were restrained from moving along the y-direction on both the bottom and top sides.

Also, the plate was to expand along the x-direction (fig. 3(d)). This was imposed to simulate the gripping conditions of the plate during the experiment. An additional constraint was imposed along the z-axis to suppress rigid-body motion.

The improvement in stress level for the two analytical cases considered, with and without air cooling, is indicated in both figures 10(a) and (b) by the fact that the maximum stress dropped about 20 percent from a maximum of 179 MPa to a low of 145 MPa. This confirms that cooling will help reduce the stresses. Also, it should be noted that the highest stress region was confined to the upper section of the plate and, in particular, the upper corner edge above the largest cooling channel. Further, this leads to a likely cracking of the coating if these stresses were to exceed the material's yield strength. Both the high temperature and the bending stresses caused by the heat are the primary drivers for these high stresses. Figure 11 shows the displacement profile produced by the stress analysis and the maximum displacement experienced by the cooling plate panel due to the applied loading. It is obvious that the upper section of the plate experiences the maximum deflection, which coincides with the experiment's applied loading conditions.

CONCLUSIONS

A parametric study using the finite element method was carried out to analyze a prototype cooling-plate panel specimen. Two- and three-dimensional finite element analyses were performed under thermal loading conditions. The size and shape of the cooling holes were varied, and the corresponding temperature profiles were calculated. The effects of the cooling channels and the coolant on both the thermal and the stress responses were investigated. The following conclusions were drawn:

1. The analyses showed that the cooling channels have substantial effects on the thermal profile. A temperature drop of 204 °C resulted when the plate was air cooled.

2. Cooling channel shape seems to have influenced the temperature level; the ascending order size arrangement performed the best by attaining the lowest temperature (1077 °C) in comparison to the circular (1379 °C) and rectangular (1343 °C) channels for the same cooling hole size. This led to the conclusion that the panel with the ascending order cooling channels remains attractive regardless of the complexity involved in its manufacturability.

3. The computed tomography scan data offered detailed information regarding hidden anomalies and manufacturing nonuniformities, which assisted greatly in the finite element modeling of nonmanufacturing components. TBC effects were noticed by limiting the high-temperature profile to a thin layer at the top of the plate.

4. Further studies are planned to include wider coverage of the effects of key parameters, such as material surface roughness, TBC/EBC, and coolant pressure differential with more representative thermal boundary conditions. Later stages of these activities will include analyzing conventional shapes of essential engine components.

REFERENCES

1. Bhatt, R.T.: Minimally Cooled Ceramics and Fiber Reinforced Ceramic Matrix Composite Turbine Components: A Progress Report. NASA/CP—1999-208915, 1999. Available from the Subsonic Systems Office, NASA Glenn Research Center.
2. Engineering Property Data on Selected Ceramics, Vol. 1: Nitrides, MCIC–HB–07, Battelle Columbus Laboratories, Columbus, OH, 1981.
3. Engineering Property Data on Selected Ceramics, Vol. 3: Single Oxides, MCIC–HB–07, Battelle Columbus Laboratories, Columbus, OH, 1981.
4. Richerson, D.W.: Modern Ceramics Engineering: Properties, Processing and Use in Design. Marcel Dekker, Inc., New York, NY, 1982.
5. MSC/PATRAN Graphics and Finite Element Package. Vols. I and II. The MacNeal-Schwendler Corporation, 1997, Costa Mesa, CA, 1997.
6. MARC General Purposes Finite Element Analysis Program. Vol. A: User Information Manual; Vol. F: Theoretical Manual. MARC Analysis Research Corporation, Palo Alto, CA, 1996.
7. ANSYS Finite Element Program. ANSYS Release 5.4, ANSYS, Inc., Canonsburg, PA, 1997.
8. Wolf, H.: Heat Transfer, Harper & Row, New York, NY, 1983, p. 3.

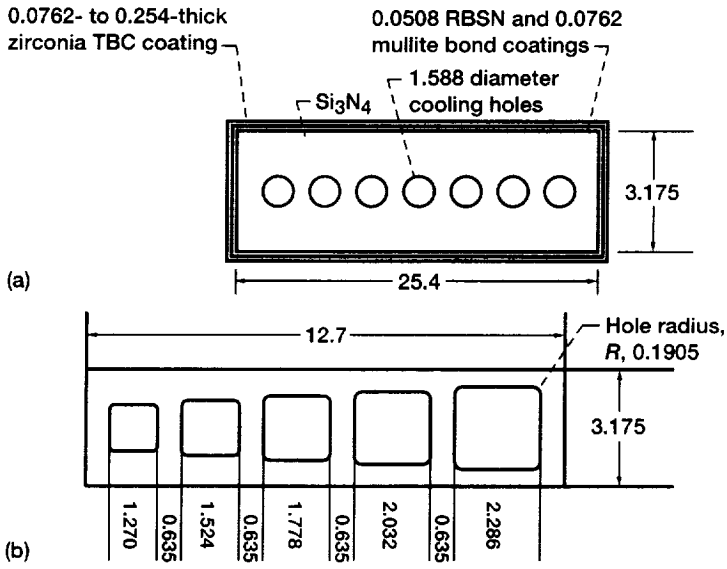

Figure 1.—Conceptual design of TBC-cooled monolithic silicon nitride (Si_3N_4) plate with cooling channels. (a) Cross-sectional view of a plate test specimen with circular cooling channels. (Cooling panel size, 125.4 by 25.4 by 3.175.) (b) Cross section of a plate containing square holes of varying sizes. All dimensions given in millimeters.

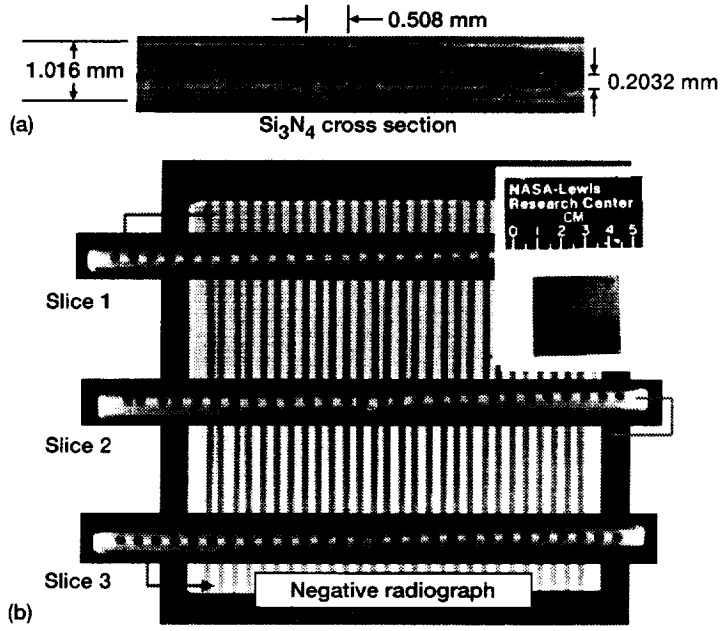

Figure 2.—Cross sections of a cooled silicon nitride panel. (a) Optical photograph of the cross section of a silicon nitride plate with cooling holes. (b) Computed tomographic image and cross-sectional view at three different locations showing inhomogeneity in cooling hole shape and spacing as well as cracks in the walls of the cooling holes.

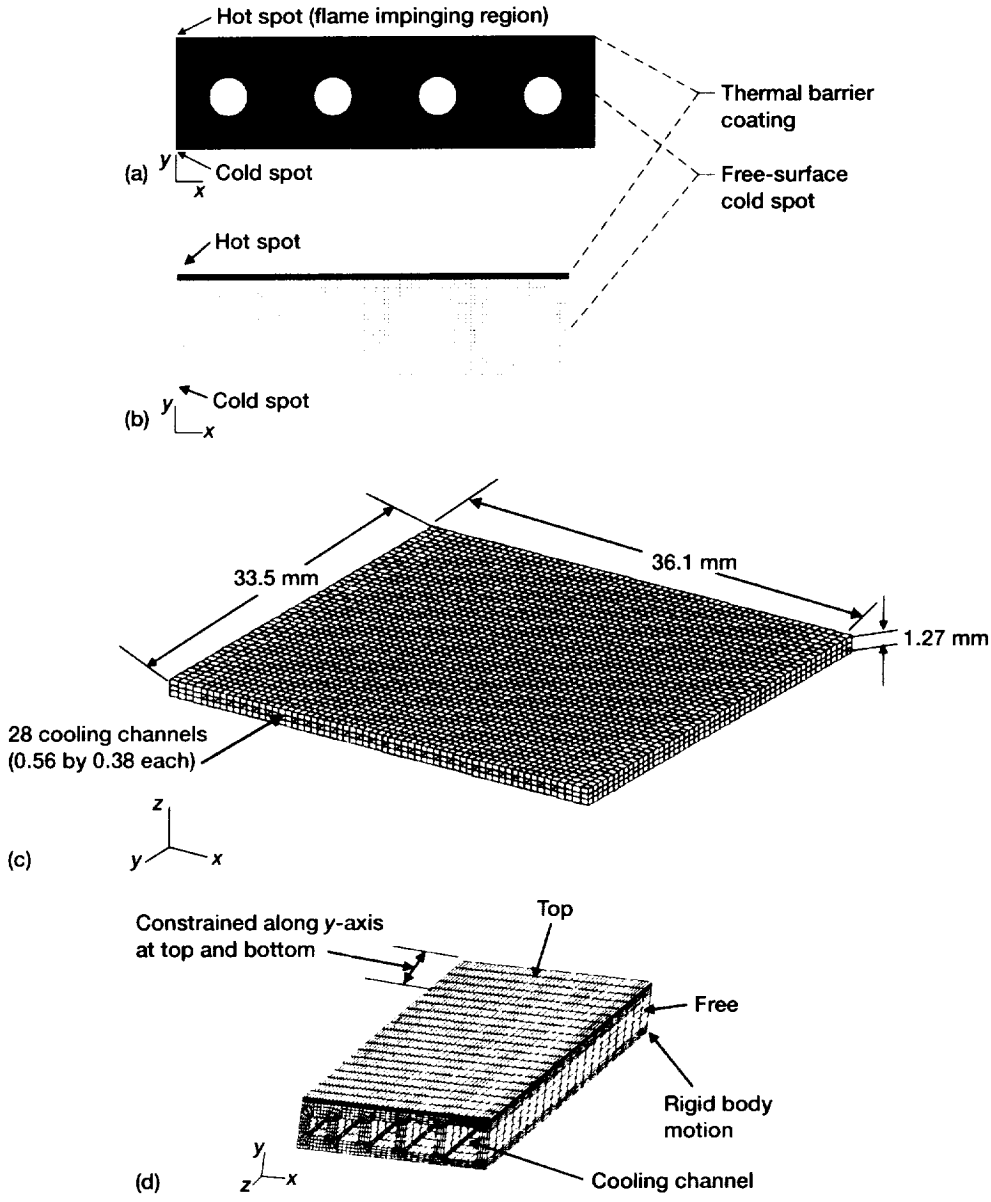

Figure 3.—Specimen geometry used for finite element modeling. (a) Circular cooling channels. (b) Rectangular cooling channels. (c) Panel shown in figure 1; 8372 eight-node brick elements and 13,568 nodes. (d) Ascending channel size, 17,760 elements and 21,546 nodes.

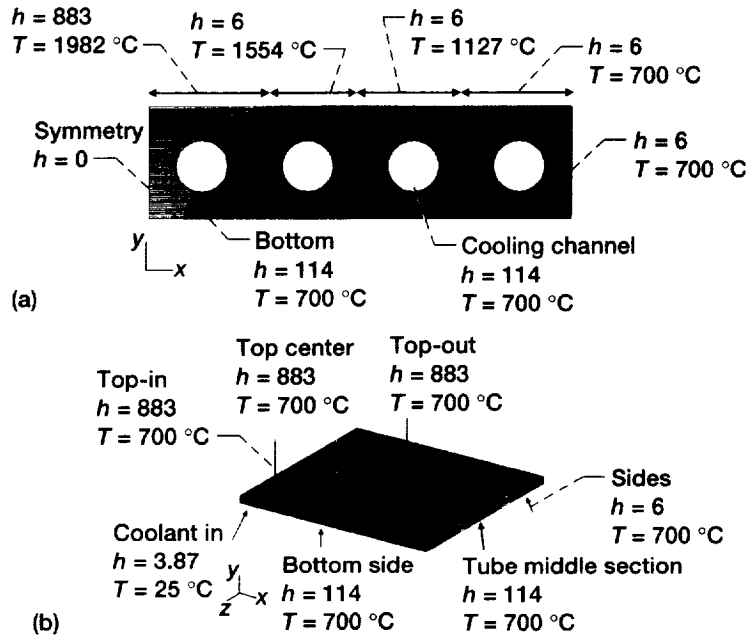

Figure 4.—Thermal boundary conditions showing applied gas temperature and heat transfer coefficient, h which is given in watts per square meters degree Celsius (W/m^2–°C). (a) Two-dimensional model. (b) Three-dimensional model.

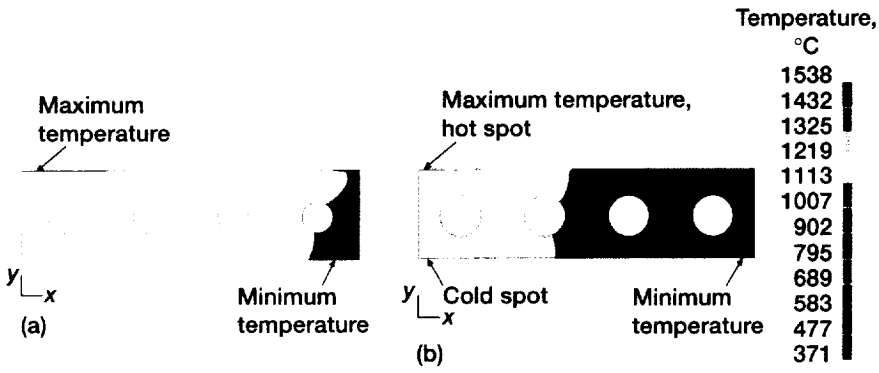

Figure 5.—Influence of cooling hole diameter on predicted ANSYS temperature distribution for Si_3N_4 plate internally cooled with air. (a) Hole radius, R, 1.143 mm. (b) Hole radius, R, 1.524 mm.

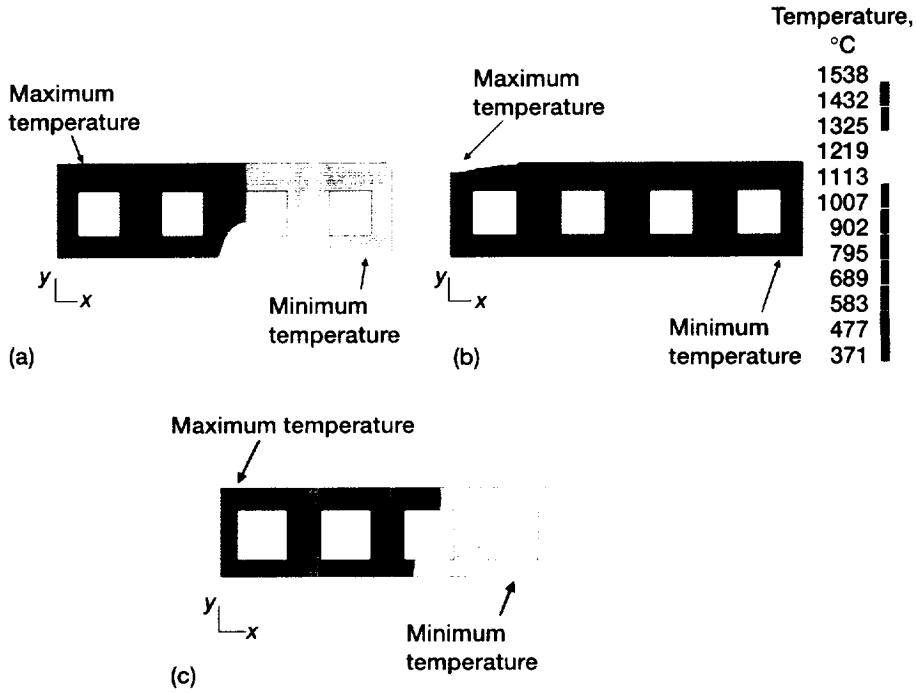

Figure 6.—Two-dimensional finite element ANSYS heat transfer analysis. Influence of cooling on temperature distribution. (a) No air cooling; square hole side, R, 1.559 mm. (b) Air cooling; square hole side, R, 1.559 mm. (c) No air cooling; square hole side, R, 1.871 mm.

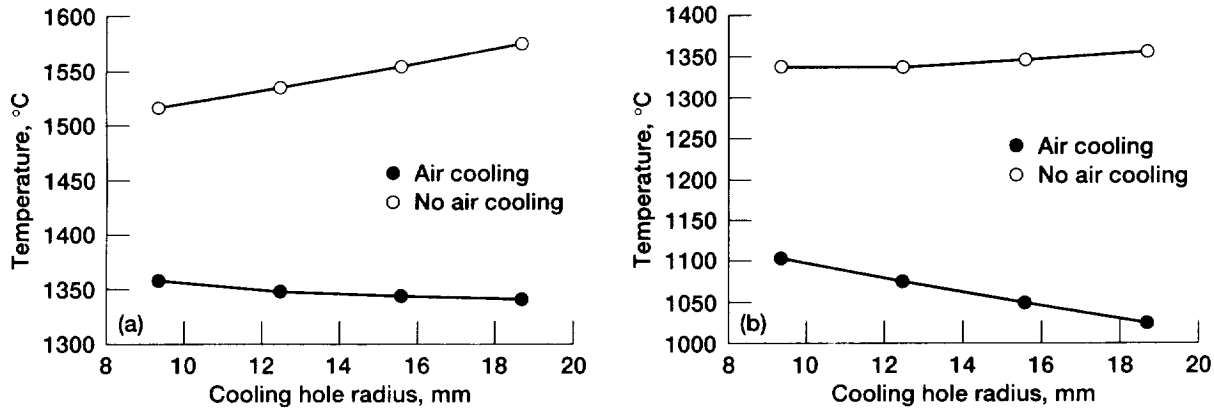

Figure 7.—Temperature variation as a function of hole size. (a) Hot spot temperature. (b) Cold spot temperature.

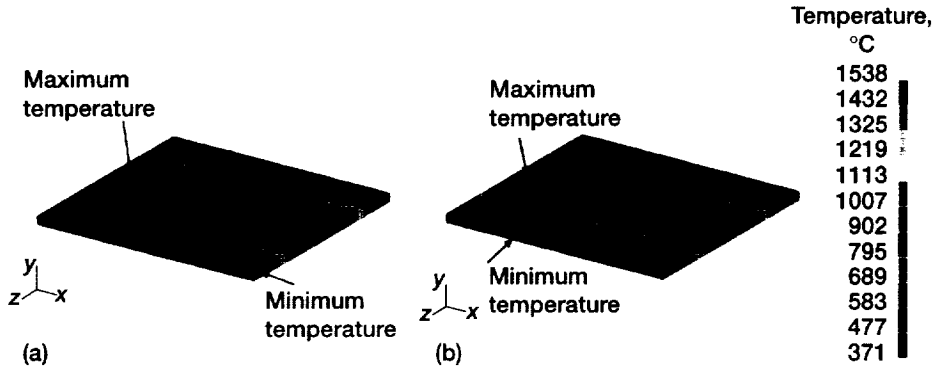

Figure 8.—Temperature distribution. (a) No air cooling. (b) Air cooling (see fig. 3 for hole sizes and shapes).

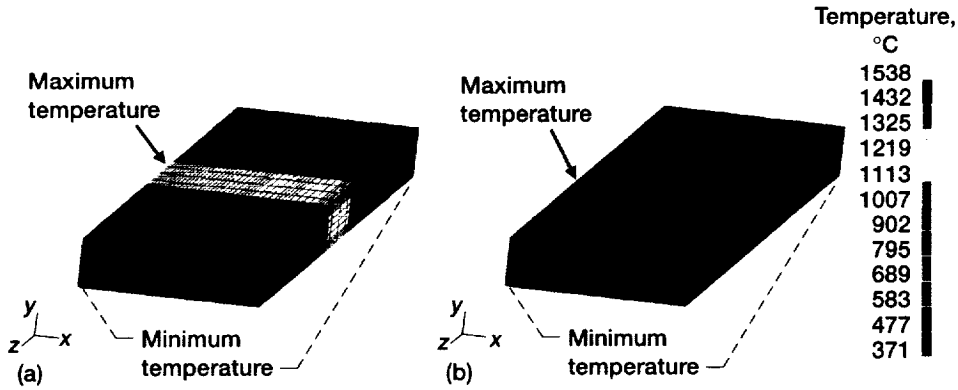

Figure 9.—Temperature distribution. (a) No air cooling. (b) Air cooling.

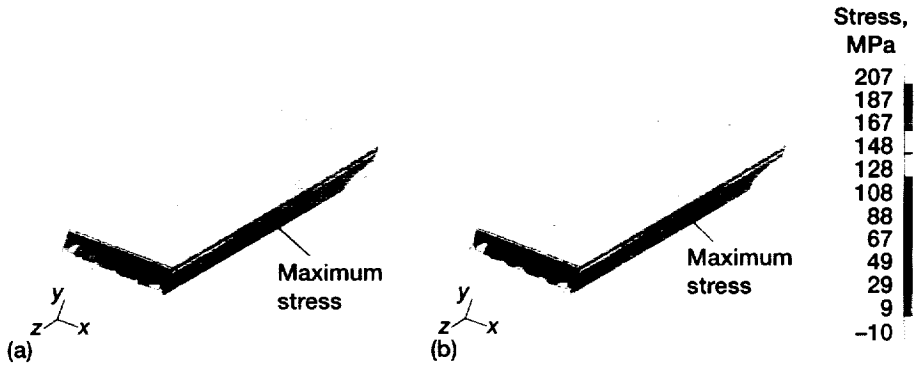

Figure 10.—Maximum principal stress distribution. (a) No air cooling. (b) Air cooling.

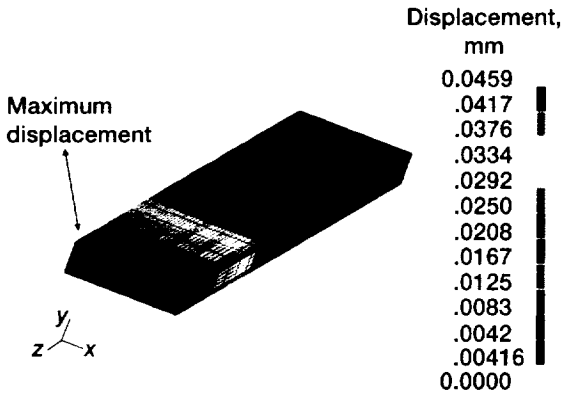

Figure 11.—Displacement profile with air cooling.

REPORT DOCUMENTATION PAGE

Form Approved
OMB No. 0704-0188

Public reporting burden for this collection of information is estimated to average 1 hour per response, including the time for reviewing instructions, searching existing data sources, gathering and maintaining the data needed, and completing and reviewing the collection of information. Send comments regarding this burden estimate or any other aspect of this collection of information, including suggestions for reducing this burden, to Washington Headquarters Services, Directorate for Information Operations and Reports, 1215 Jefferson Davis Highway, Suite 1204, Arlington, VA 22202-4302, and to the Office of Management and Budget, Paperwork Reduction Project (0704-0188), Washington, DC 20503.

1. AGENCY USE ONLY (*Leave blank*)	2. REPORT DATE	3. REPORT TYPE AND DATES COVERED
	June 2001	Technical Memorandum

4. TITLE AND SUBTITLE

Design Evaluation Using Finite Element Analysis of Cooled Silicon Nitride Plates for a Turbine Blade Application

5. FUNDING NUMBERS

WU–708–31–13–00

6. AUTHOR(S)

Ali Abdul-Aziz, George Y. Baaklini, and Ramakrishna T. Bhatt

7. PERFORMING ORGANIZATION NAME(S) AND ADDRESS(ES)

National Aeronautics and Space Administration
John H. Glenn Research Center at Lewis Field
Cleveland, Ohio 44135–3191

8. PERFORMING ORGANIZATION REPORT NUMBER

E–12735

9. SPONSORING/MONITORING AGENCY NAME(S) AND ADDRESS(ES)

National Aeronautics and Space Administration
Washington, DC 20546–0001

10. SPONSORING/MONITORING AGENCY REPORT NUMBER

NASA TM—2001-210819

11. SUPPLEMENTARY NOTES

Prepared for the 103rd Annual Meeting and Exposition sponsored by The American Ceramic Society, Indianapolis, Indiana, April 22–25, 2001. Ali Abdul-Aziz, Cleveland State University, 1983 E. 24th Street, Cleveland, Ohio 44115–2403 (NASA Resident Research Associate at Glenn Research Center); George Y. Baaklini, NASA Glenn Research Center; Ramakrishna T. Bhatt, U.S. Army Research Laboratory, Glenn Research Center, Cleveland, Ohio 44135. Responsible person, Ali Abdul-Aziz, organization code 5920, 216–433–6729.

12a. DISTRIBUTION/AVAILABILITY STATEMENT

Unclassified - Unlimited
Subject Categories: 01 and 39 Distribution: Nonstandard

Available electronically at http://gltrs.grc.nasa.gov/GLTRS

This publication is available from the NASA Center for AeroSpace Information, 301–621–0390.

12b. DISTRIBUTION CODE

13. ABSTRACT ***(Maximum 200 words)***

Two- and three-dimensional finite element analyses were performed on a prototype plate specimen with cooling holes made of ceramic materials. Steady-state heat-transfer analyses were done to evaluate the thermal environment experienced by the specimen and to optimize the size of the cooling holes and the geometry of the cooling channels to reduce thermal stresses and burner rig testing. The limited experimental data available were used to model the thermal profile exerted by the flame on the plate. Thermal stress analyses were made to evaluate the stress response due to thermal loading. Contours for the temperature and the representative stresses for the specimen were generated and presented for different cooling hole sizes and shapes. The thermal barrier coating experienced high stresses, and the temperature gradient was much reduced when cooling holes were used. The advantages and disadvantages of several cooling channel layouts were evaluated.

14. SUBJECT TERMS

Ceramics; Finite element; Cooling plates; Silicon nitrides; Thermal stress analysis

15. NUMBER OF PAGES

21

16. PRICE CODE

17. SECURITY CLASSIFICATION OF REPORT	18. SECURITY CLASSIFICATION OF THIS PAGE	19. SECURITY CLASSIFICATION OF ABSTRACT	20. LIMITATION OF ABSTRACT
Unclassified	Unclassified	Unclassified	